*International Journal of Minerals, Metallurgy and Materials*
*Volume 21, Number 5, May 2014, Page 479*
**DOI: 10.1007/s12613-014-0932-7**

# Microstructure and mechanical properties of spark plasma sintered Ti–Mo alloys for dental applications

*Xin Lu*[1,2], *Bo Sun*[2], *Teng-fei Zhao*[2], *Lu-ning Wang*[2], *Cheng-cheng Liu*[2], *and Xuan-hui Qu*[1,2]

1) State Key Laboratory for Advanced Metals and Materials, University of Science and Technology Beijing, Beijing 100083, China
2) School of Materials Science and Engineering, University of Science and Technology Beijing, Beijing 100083, China
(Received: 8 September 2013; revised: 7 December 2013; accepted: 22 December 2013)

**Abstract:** Ti–Mo alloys with various Mo contents from 6wt% to 14wt% were processed by spark plasma sintering based on elemental powders. The influence of sintering temperature and Mo content on the microstructure and mechanical properties of the resulting alloys were investigated. For each Mo concentration, the optimum sintering temperature was determined, resulting in a fully dense and uniform microstructure of the alloy. The optimized sintering temperature gradually increases in the range of 1100–1300°C with the increase in Mo content. The microstructure of the Ti–(6–12)Mo alloy consists of acicular α phase surrounded by equiaxed grains of β phase, while the Ti–14Mo alloy only contains single β phase. A small amount of fine α lath precipitated from β phase contributes to the improvement in strength and hardness of the alloys. Under the sintering condition at 1250°C, the Ti–12Mo alloy is found to possess superior mechanical properties with the Vickers hardness of Hv 472, the compressive yield strength of 2182 MPa, the compression rate of 32.7%, and the elastic modulus of 72.1 GPa. These results demonstrate that Ti–Mo alloys fabricated via spark plasma sintering are indeed a perspective candidate alloy for dental applications.

**Keywords:** titanium alloys; spark plasma sintering; microstructure; mechanical properties

## 1. Introduction

Titanium and titanium alloys are considered to be one of the most attractive materials for orthodontic applications due to their low density, excellent biocompatibility, good mechanical properties, and incredible corrosion resistance [1–2]. Because of the potential toxicity of Al and V, however, titanium-based alloys such as Ti–6Al–4V, Ti–5Al–2.5Fe, and Ti–6Al–7Nb (wt%) are unsuitable for biomedical applications. In addition, the elastic moduli of implant materials are still much higher than the modulus of cortical bone. The stress shielding effect derived from this mismatch may lead to implant failure [3–4]. Consequently, extensive effort has been expended to design new β-Ti alloys with a low elastic modulus and nontoxic alloying elements. Among β stabilizer elements, such as Zr, Nb and Mo, Mo is recognized as one of the most effective β stabilizers when added to an alloy in small quantities [5]. The addition of Mo tends to stabilize β phase and decreases the elastic modulus of the alloys. Moreover, Mo is a refractory element with a high melting point, and the addition of Mo can also enhance the strength and abrasion resistance of Ti-based alloys. Binary Ti–Mo alloys with Mo contents of 5wt%–20wt% have been developed, and these previous studies have demonstrated that the alloys exhibit reliable mechanical and corrosion performance and are promising for use in orthodontic applications [5–9].

Ti–Mo alloys are usually prepared by casting and subsequent thermomechanical treatment. However, this fabrication technique suffers some drawbacks, such as expensive thermomechanical treatment, unavoidable machining, and associated materials loss. In comparison, a cost-effective technique of powder metallurgy (PM) can be used to produce complex-shaped Ti-alloy components. This fabrication process provides a convenient method of adding alloying elements and results in production with a high degree of chemical homogeneity and fine grain size; in addition, PM allows the fabrication of porous materials.

As one of the novel powder metallurgy techniques, spark plasma sintering (SPS) can effectively produce a fine-

Corresponding author: Xuan-hui Qu E-mail: quxh@ustb.edu.cn

grained material in a short duration. Previous studies have demonstrated that Ti alloys for biomedical applications can be prepared by SPS [10–14], however, few of these studies have involved the systematic examination of relationships between the processing parameters, Mo content, microstructure, and mechanical properties of binary Ti–Mo alloys.

In the present study, dense and uniform Ti–Mo alloys with various microstructural characteristics were fabricated from elemental powders via SPS. The effect of processing parameters and Mo content on the microstructure and mechanical properties of the materials were systematically investigated.

## 2. Experimental

Elemental powders of Ti (purity 99.9%, <45 μm) and Mo (purity 99.9%, <45 μm) were used as raw materials. Powder mixtures with different Mo contents (6wt%–14wt%) were mechanically mixed for 6 h. The premixed powder was poured into a graphite die, which was plugged at both ends with graphite punches; the die assembly was subsequently placed in a SPS furnace (DR SINTERING-1050). Samples were warmed to the sintering temperature at a heating rate of 100°C/min under a vacuum of 2 Pa and then sintered from 900°C to 1350°C for 5 min under a pressure of 40 MPa. Finally, the sintered samples were furnace-cooled to room temperature. The temperature was monitored using a W–Re thermocouple, which measured the temperature of the graphite die. The sintered samples were disk-shaped with a diameter of 20 mm and a height of ~8 mm. Several cylindrical samples were machined to a gauge size of ϕ4 mm × 6 mm for compression testing.

Samples were polished and etched in a solution of Kroll's reagent, which contained the distilled water, nitric acid, and hydrofluoric acid (85:15:5 by volume). The surface morphology and microstructure of samples were examined by scanning electron microscopy (SEM, LEO1450). The density of samples was determined by the Archimedes' drainage method. X-ray diffraction (XRD) was used to characterize phases in the resultant samples. Hardness tests were conducted on a Rockwell and Vickers hardness tester, respectively. For the intrinsic hardness measurements, all the samples were polished with 1500-grit SiC grinding papers. The Rockwell hardness was measured under a load of 1.5 N for a holding time of 10 s. Mechanical compression tests were performed on an Instron machine at a strain rate of $2 \times 10^{-3}$ $s^{-1}$ at room temperature. The compression ratio and compressive elastic modulus were deduced from the stress–strain curves.

## 3. Results and discussion

### 3.1. Effect of sintering temperature on microstructure and properties

3.1.1. Density

Fig. 1 shows the variation in density of samples with respect to sintering temperature and Mo content. The density of samples strongly depends on both sintering temperature and Mo content. In general, at the same Mo content, the density rapidly increases with increasing sintering temperature and then tends to stabilize at a level close to the theoretical density of the alloys (i.e., the density of the as-cast alloys). With increasing Mo content, the sample density substantially increases, and the minimum sintering temperature corresponding to the density at the steady-state distinctly increases. In the case of the Ti–6Mo alloy, the density stabilizes at approximately 4.713 g/cm$^3$ at or above the sintering temperature of 1100°C, at approximately 4.831 g/cm$^3$ at or above 1200°C for the Ti–10Mo alloy, and at 4.961 g/cm$^3$ at or above 1300°C for the Ti–14Mo alloy.

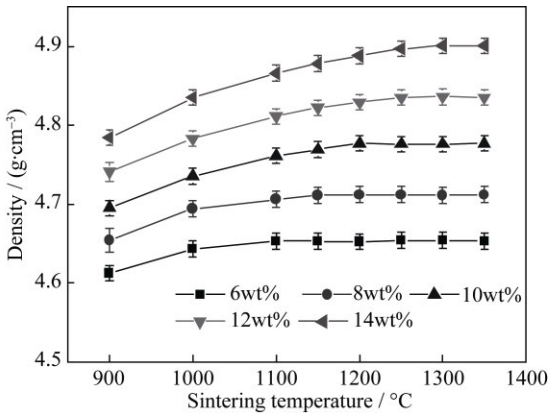


**Fig. 1. Influence of sintering temperature on the density of samples with different Mo contents.**

3.1.2. Rockwell hardness

Fig. 2 shows the Rockwell hardness values of the sintered samples with different Mo contents at different sintering temperatures. Because of the microstructural inhomogeneity of samples, Rockwell hardness was preferentially used for all the samples instead of Vickers measurements. Notably, sintering temperature and Mo content strongly influence the hardness of samples. Samples sintered at 1000°C exhibit the lowest hardness, and their hardness varies little with different Mo contents. For samples with a fixed Mo content, the hardness first rapidly increases and then decreases after the peak hardness as the sintering temperature increases. The peak hardness values initially increase with the increase of Mo content from HRC 40.5 (Ti–6Mo) to HRC 46.5

(Ti–12Mo), and then decrease to HRC 44.1 when the Mo content further increases to 14wt%. In general, the increase in hardness of Ti–Mo alloys can be attributed to an enhanced solid solution strengthening effect induced by the addition of Mo. The crystal structure, grain size, phase morphology, and precipitation hardening can all affect the hardness of the alloys. Notably, the sintering temperature at the peak hardness gradually increases with increasing Mo content, which is consistent with the minimum sintering temperature required to achieve a stable density. For Ti–Mo alloys with Mo contents of 6wt%, 8wt%, 10wt%, 12wt%, and 14wt%, the sintering temperatures, at which the maximum density and hardness are achieved, are 1100, 1150, 1200, 1250, and 1300°C, respectively.

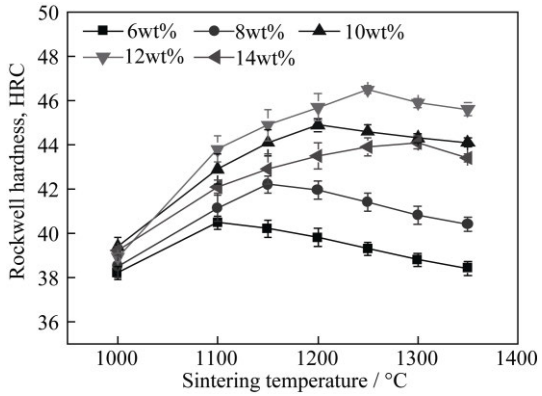


**Fig. 2. Influence of sintering temperature on the Rockwell hardness of samples with different Mo contents.**

3.1.3. Microstructure

Fig. 3 shows the XRD patterns of Ti–10Mo alloy samples sintered at different temperatures. The clear diffraction peaks suggest that the samples have similar phase compositions and mainly consist of α and β phases. With the increase of sintering temperature, the intensities of XRD peaks for β phase tend to increase slightly.

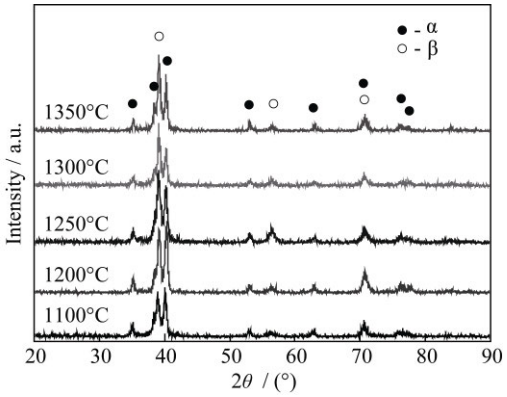


**Fig. 3. XRD patterns of Ti–10Mo alloy samples sintered at different temperatures.**

Fig. 4 displays the SEM micrographs of Ti–10Mo alloy samples sintered at different temperatures. Notably, the samples sintered at 1150–1300ºC are nearly fully dense, with no obvious pores. The samples sintered at 1150ºC exhibit an inhomogeneous microstructure, where the alloying element, Mo, is incompletely dissolved (bright zones), and acicular α phase (gray) is dispersed in grains of β phase, as shown in Figs. 4(a) and (b). In the cases of Ti–10Mo alloy samples sintered at or above 1200°C, a homogeneous microstructure is obtained, consisting of β phase and fine acicular α phase. This result is consistent with the density results. In addition, the β phase grains gradually grow with increasing sintering temperature. Whereas the acicular α phase tends to be fine when the sintering temperature is 1200°C or less, it shows little variation in the samples sintered above 1200°C.

Maintaining at the experimental sintering temperatures, Ti–10Mo alloy samples were in the β single-phase region, where Mo diffused into the titanium matrix. During furnace cooling, β phase grains were subjected to the precipitation of acicular α phase along grain boundaries and in the transgranular because of high cooling rate. The diffusing rate of Mo (the β stabilizing alloying element) increased with the increase of sintering temperature. Therefore, the Mo content of β phase was gradually elevated with temperature until the diffusion process was completed in the samples maintained at or above 1200°C. A higher Mo content in β phase grains made the precipitation of acicular α phase more difficult. Therefore, the grains of β phase became coarser with the finer α lath in them, when the sintering temperature increased. When the sintering temperature was greater than 1200°C, the microstructural feature of α phase showed little variation because the Mo content in β phase grains reached a steady state. In the case of the Ti–10Mo alloy, a homogeneous microstructure and relatively fine grains could be obtained by spark plasma sintering at 1200°C, corresponding to the maximum density and hardness testing results, respectively. According to the test results, the other Ti–Mo alloys showed a trend similar to that of Ti–10Mo. Their optimum sintering temperatures were 1100°C (Ti–6Mo), 1150°C (Ti–8Mo), 1250°C (Ti–12Mo), and 1300°C (Ti–14Mo). These samples were used in subsequent analyses.

### 3.2. Effect of Mo content on properties and microstructure

3.2.1. Microstructure

The XRD patterns of samples with different Mo contents are shown in Fig. 5. The intensity of diffraction peaks for β

phase increases substantially with the increase of Mo content. Except for the Ti–14Mo alloy containing just β phase, the other spark-sintered binary Ti–Mo alloys all consist of mixed α and β phases. This difference is caused by the β stabilizing action of Mo. Because of their lower Mo contents, the Ti–6Mo and Ti–8Mo alloys are primarily composed of α phase with a small amount of residual β phase. With increasing Mo content, the volume fraction of β phase increases significantly. When the Mo content is 12wt%, the formation of α phase is largely suppressed, and the alloy is dominated by β phase. When the Mo content is 14wt%, only the residual β phase is observed in the XRD patterns.

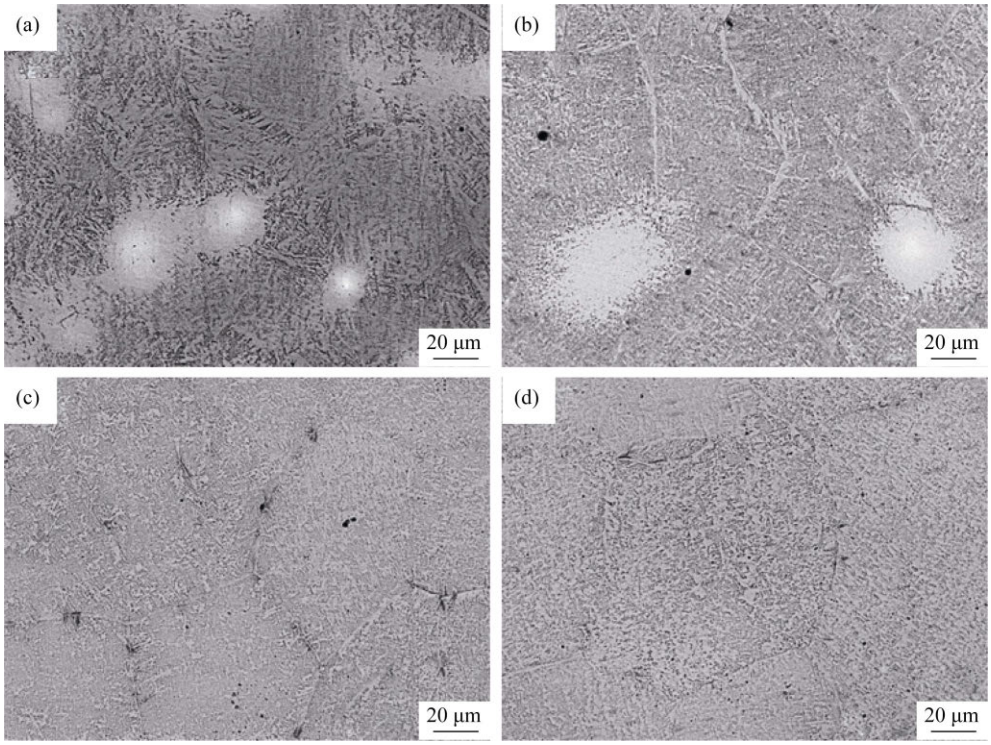


**Fig. 4. Microstructures of Ti–10Mo alloy samples sintered at different temperatures: (a) 1100°C; (b) 1150°C; (c) 1200°C; and (d) 1250°C.**

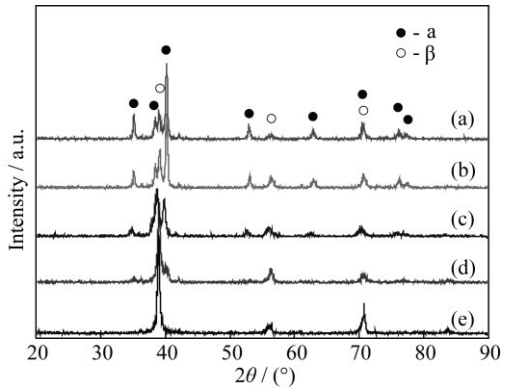


**Fig. 5. XRD patterns of samples with different Mo contents: (a) 6wt% (sintering temperature 1100°C); (b) 8wt% (1150°C); (c) 10wt% (1200°C); (d) 12wt% (1250°C); (e) 14wt% (1300°C).**

Fig. 6 shows the SEM micrographs of samples with different Mo contents. Ti–(6–14)Mo alloys with a high relative density and uniform microstructures can be obtained by SPS at sintering temperatures of 1100, 1150, 1200, 1250, and 1300°C. Mo content strongly influences the microstructures of binary Ti–Mo alloys. Samples with Mo contents of 6wt% and 8wt% exhibit the similar microstructures, which consist of the equiaxed grains of β phase and the multiple variants of α lath, as shown in Figs. 6(a) and (b). When the Mo content reaches 10wt%, the size of α lath within β phase grains decreases substantially, as shown in Fig. 6(c). When the Mo content is 12wt%, the amount of α lath obviously decreases, and the α lath is mainly dispersed along the grain boundaries of β phase (Fig. 6(d)). Fig. 6(e) shows that a microstructure consisting of the equiaxed grains of β phase is obtained for samples containing of 14wt% Mo. In addition, no distinct change in size of β phase grains is observed in the case of samples with different Mo contents.

From the aforementioned results, the sintering temperature required to yield a relatively high-density and uniform microstructure gradually increased with the increase of Mo content, because an increase in Mo content not only increased the melting points of binary Ti–Mo alloys but also caused a sharp decrease in the interdiffusion coefficients of

Ti–Mo alloys [15–16]. Thus, achieving a uniform diffusion of chemical constituents within the same holding time required a higher sintering temperature. In addition, a high Mo content made the precipitation of α phase more difficult due to the β stabilizing action of Mo, leading to a decrease in the content and size of α lath. An increase in sintering temperature did not induce the significant growth of β phase grains, which was believed to be a consequence of Mo-grain boundary interactions, which slowed down the growth of grain boundaries.

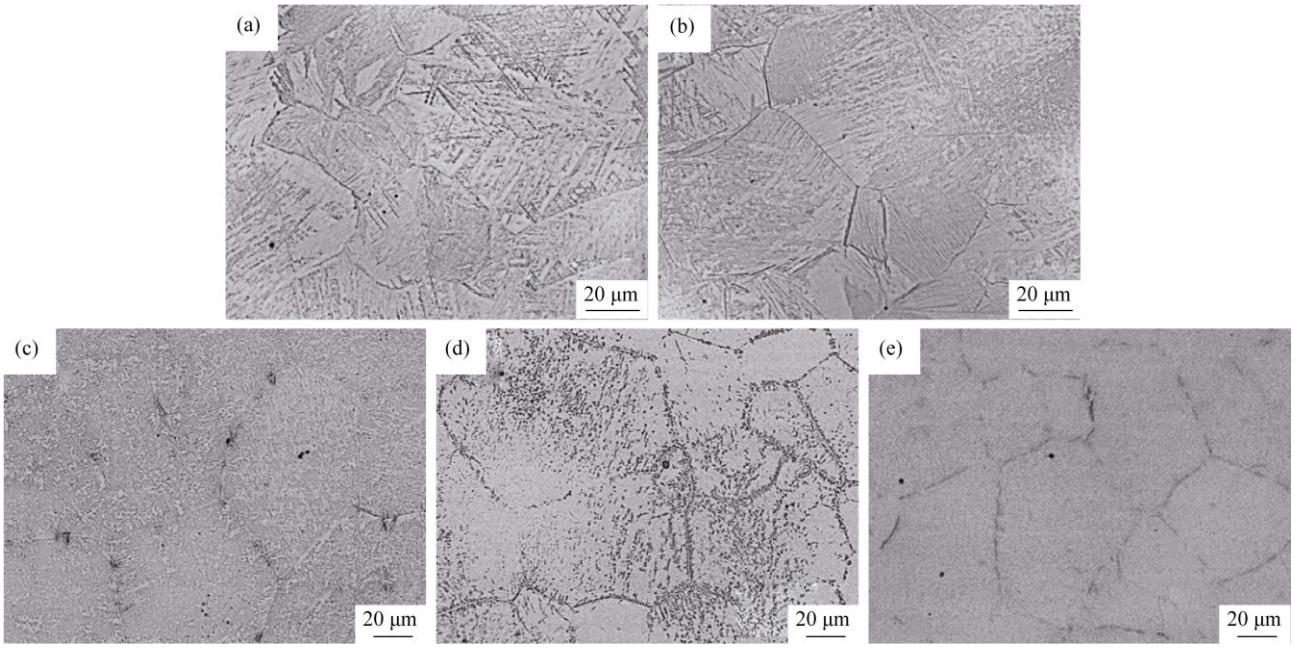


**Fig. 6. Microstructures of samples with different Mo contents: (a) 6wt% (sintering temperature 1100°C); (b) 8wt% (1150°C); (c) 10wt% (1200°C); (d) 12wt% (1250°C); (e) 14wt% (1300°C).**

3.2.2. Vickers hardness

The Vickers hardness of sintered samples with different Mo contents is shown in Fig. 7. The results are essentially consistent with the Rockwell hardness test results. All the as-SPSed Ti–Mo alloy samples with 6wt%–14wt% Mo obviously have much higher microhardness values (Hv 396–472) than Ti–6Al–4V alloys processed by cast (Hv 294) [7] or powder metallurgy techniques (Hv 350) [17]. Among the investigated samples, the Ti–12Mo alloy dominated by fine β phase grains exhibits the highest Vickers hardness value of Hv 472, which is significantly higher than that of the as-cast Ti–12.5Mo alloy (Hv 350) [7] due to the finer grain size of the Ti–12Mo alloy.

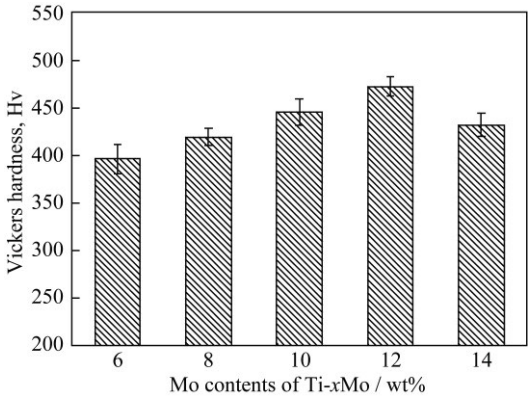


**Fig. 7. Vickers hardness of samples with different Mo contents.**

3.2.3. Room-temperature mechanical properties

Fig. 8 shows the compressive properties of binary Ti–Mo alloy samples with different Mo contents, including the ultimate compressive strength (UCS), yield strength (YS), compression ratio (CR), and Young's elastic modulus. As evident from the results, Mo content substantially affects the room temperature mechanical properties of the alloys. Overall, the as-SPSed Ti–(6–14)Mo alloys exhibit superior mechanical strength with the ultimate compressive strength of approximately 3 GPa. The variation trend of strength with the increase of Mo content is similar to that of hardness. The compressive strengths initially increase with increasing Mo content when the Mo content is less than 12wt%, and then decrease in the samples with 14wt% Mo. In comparison, the Ti–12Mo alloy exhibits the highest strength with the ultimate compressive strength of 3413 MPa and the yield strength of 2182 MPa. The Ti–10Mo and Ti–14Mo alloys exhibit the similar strengths, and their ultimate and yield strengths are approximately 3100 MPa and 1800 MPa, re-

spectively. The compression ratios of Ti–*x*Mo alloys decrease from 27.8% to 26.3% when the Mo content is increased from 6wt% to 8wt%. With a further increase in Mo content of 8wt% to 14wt%, the compressive ductility gradually ascends. Consequently, the Ti–14Mo alloy exhibits the greatest ductility with the compressive ratio of 33.1%; the compressive ratios of Ti–12Mo and Ti–10Mo are 32.7% and 30.4%, respectively. Furthermore, the Young's elastic modulus of the as-SPSed Ti–*x*Mo alloys slightly decrease from 71 GPa to 85 GPa as the Mo content increases. The Ti–14Mo alloy exhibits the lowest compressive modulus of 71.4 GPa, similar to the modulus of 72.1 GPa for Ti–12Mo.

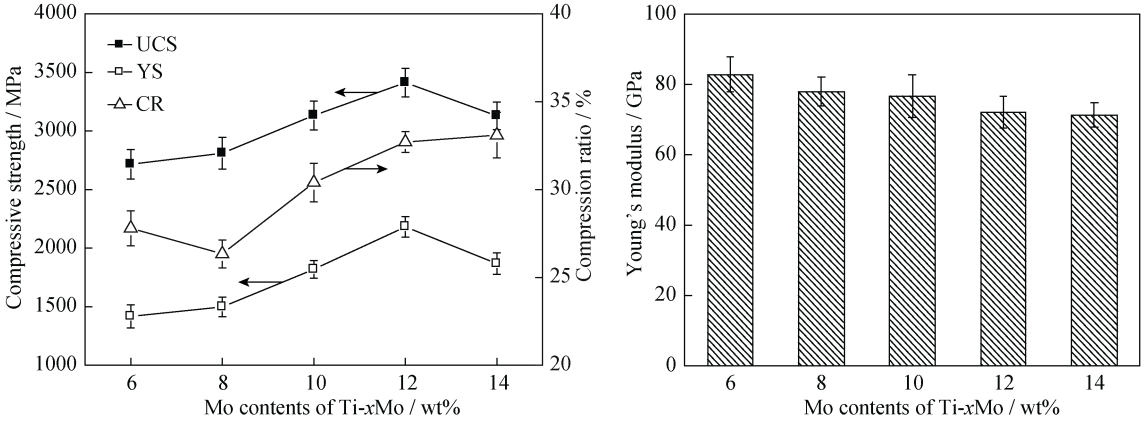


**Fig. 8. Compressive properties of samples with different Mo contents.**

The mechanical properties of Ti-based alloys at room temperature strongly depend on their microstructures, including grain size, the volume fraction of β phase, and the morphology of precipitated α phase. In the case of Ti–Mo alloys with low Mo contents of 6wt% or 8wt%, the microstructures mainly consist of massive coarse α lath and β phase grains. The coarse and long α lath microstructure provides a smooth route for crack propagation, leading to a relatively high growth rate of fatigue cracks. In addition, the coarse lath may make the dislocation slip more difficult during the deformation process, and the cleavage fracture tends to occur prematurely due to the formation of dislocation pile-up. Thus, the Ti–6Mo and Ti–8Mo alloys exhibit lower compressive strength and ductility. Compared to the Ti–6Mo alloy, the Ti–8Mo alloy exhibits greater strength but lower ductility, which is perhaps caused by the effect of β/α interface. The increase in Mo content causes the volume fraction of β phase to increase, thereby leading to the enhanced effect of β/α interface. The β/α interface microstructure contributes to the obstruction of slip bands. Therefore, the strength increases and the ductility decreases.

In the case of the Ti–Mo alloy with 10wt% Mo, the microstructures consist of massive finer α lath and β phase grains. Compared with the Ti–6Mo and Ti–8Mo alloys, the Ti–10Mo alloy exhibits greater strength and ductility. The improvements in these properties are attributable to the substantial decrease in the size of α lath in the Ti–10Mo alloy. When the Mo content reaches 12wt%, the microstructure is dominated by β phase and a small amount of α lath. Because of the high plasticity and strong solid solution effect of the β phase structure, both the ductility and strength of the Ti–12Mo alloy are greater than those of the Ti–(6–10)Mo alloys. Because the Ti–14Mo alloy is characterized by equiaxed grains of β phase, as indicated by the effect of the volume fraction of β phase alone, the Ti–14Mo alloy should exhibit the highest relative strength and ductility. However, experimentally, the Ti–14Mo alloy exhibits greater compressive ductility but lower strength than that of the Ti–12Mo alloy. The increased strength of the Ti–12Mo alloy is believed to result from the precipitation hardening of finer α lath. This finding is consistent with that of Majumdar *et al.* [18]. The α phase is sandwiched between the β matrix within each packet and gives the local plastic constraints, leading to the strengthening of samples.

As one of the intrinsic properties of materials, the elastic modulus is determined by bonding force among atoms and is more sensitive to phase/crystal structure than other factors [18]. The modulus value of a multiphase alloy is determined by the specific modulus and volume fraction of phases. Previous studies [7,19] have demonstrated that the elastic modulus of β phase in Ti–Mo alloys is lower than that of α phase. In the case of Ti–*x*Mo alloys prepared by SPS, the volume fraction of β phase significantly increases with increasing Mo content, and the Young's elastic modulus of the alloys correspondingly decreases. In comparison, the Ti–12Mo and Ti–14Mo alloys are dominated by β phase but exhibit relatively lower compressive moduli with the values of ~72 GPa; and these values are similar to that of the

Ti–13Mo alloy (75 GPa) prepared via laser-assisted synthesis [20]. The compressive moduli of the Ti–12Mo and Ti–14Mo alloys are considerably lower than that of stainless steel (~110 MPa), Co-based alloys (~210 MPa), and Ti–6Al–4V (~110 MPa) [21]. The modulus is also lower than that of as-cast Ti–Mo alloys (78–93 GPa), and the decrease is attributed to the absence of ω phase [22]. Among samples measured in the present study, the Ti–12Mo alloy sintered at 1250°C by SPS exhibits the best combination of properties with the Vickers hardness of Hv 472, the compressive strength of 3413 MPa, the compressive yield strength of 2182 MPa, the compression rate of 32.7%, and the elastic modulus of 72.1 GPa. Compared with recently developed β type Ti–Nb–Ta–Zr alloys, the Ti–Mo alloy has a slightly higher modulus, but considerably greater strength and hardness [23]. Ti–Mo alloys sintered by SPS are therefore expected to have strong potential for use in dental-implant applications.

## 4. Conclusions

(1) Ti–(6–14)Mo alloys with the high relative density and uniform microstructure can be obtained from elemental powders via SPS at sintering temperatures from 1100 to 1350°C. With increasing Mo content, the optimized sintering temperatures to achieve fully dense and uniform diffusion of Mo increase.

(2) The microstructure of samples strongly depends on Mo content. The microstructure of Ti–(6–12)Mo alloys consists of acicular α phase surrounded by equiaxed grains of β phase, whereas the Ti–14Mo alloy contains only β phase. As the Mo content is increased to 6wt%–10wt%, the volume fraction of β phase gradually increases, whereas the amount and size of α lath tends to decrease.

(3) In the case of the as-SPSed Ti–(6–14)Mo alloys, the yield strength of 1800–2182 MPa and the elastic modulus of 71–85 GPa are obtained. A small amount of fine α lath precipitated from the β phase contributes to the increased strength and hardness. At a sintering temperature of 1250°C, the Ti–12Mo alloy samples contained β phase and a small amount of fine α lath are found to exhibit a superior combination of mechanical properties as the Vickers-hardness of Hv 472, the compressive strength of 3413 MPa, the compressive yield strength of 2182 MPa, the compression rate of 32.7%, and the elastic modulus of 72.1 GPa.

## Acknowledgements

This work was financially supported by the State Key Lab of Advanced Metals and Materials, University of Science and Technology Beijing (No. 2012Z–10) and the National Natural Science Foundation of China (No. 51204015).

## References

[1] M. Long and H.J. Rack, Titanium alloys in total joint replacement: a materials science perspective, *Biomaterials*, 19(1998), No. 18, p. 1621.

[2] M. Niinomi, Mechanical properties of biomedical titanium alloys, *Mater. Sci. Eng. A*, 243(1998), No. 1-2, p. 231.

[3] E. Akman, A. Demir, T. Canel, and T. Sınmazçelik, Laser welding of Ti6Al4V titanium alloys, *J. Mater. Process. Technol.*, 209(2009), No. 8, p. 3705.

[4] T. Seshacharyulu and B. Dutta, Influence of prior deformation rate on the mechanism of β→α+β transformation in Ti–6Al–4V, *Scripta Mater.*, 46(2002), No. 9, p. 673.

[5] Y.L. Zhou and D.M. Luo, Corrosion behavior of Ti–Mo alloys cold rolled and heat treated, *J. Alloys Compd.*, 509(2011), No. 21, p. 6267.

[6] D. Kuroda, M. Niinomi, M. Morinaga, Y. Kato, and T. Yashiro, Design and mechanical properties of new β type titanium alloys for implant materials, *Mater. Sci. Eng. A*, 243(1998), No. 1-2, p. 244.

[7] W.F. Ho, C.P. Ju, and J.H. Chern Lin, Structure and properties of cast binary Ti–Mo alloys, *Biomaterials*, 20(1999), No. 22, p. 2115.

[8] J. Takekawa and N. Sakurai, Effect of the processing conditions on density, strength and microstructure of Ti–12Mo alloy fabricated by PIM process, *J. Jpn. Soc. Powder Powder Metall.*, 46(1999), No. 8, p. 877.

[9] Y. Liu, W.F. Wei, K.C. Zhou, L.F. Chen, and H.P. Tang, Microstructures and mechanical behavior of PM Ti–Mo alloy, *J. Cent. South Univ. Technol.*, 10(2003), No. 2, p. 81.

[10] Y.W. Kim, Y.J. Lee, and T.H. Nam, Shape memory characteristics of Ti–Ni–Mo alloys sintered by sparks plasma sintering, *J. Alloys Compd.*, 577(2013), Suppl. 1, p. S205.

[11] Y.Y. Li, L.M. Zou, C. Yang, Y.H. Li, and L.J. Li, Ultrafine-grained Ti-based composites with high strength and low modulus fabricated by spark plasma sintering, *Mater. Sci. Eng. A*, 560(2013), p. 857.

[12] R. Nicula, F. Lüthen, M. Stir, B. Nebe, and E. Burkel, Spark plasma sintering synthesis of porous nanocrystalline titanium alloys for biomedical applications, *Biomol. Eng.*, 24(2007), No. 5, p. 564.

[13] A. Ibrahim, F. Zhang, E. Otterstein, and E. Burkel, Processing of porous Ti and Ti5Mn foams by spark plasma sintering, *Mater. Des.*, 32(2011), No. 1, p. 146.

[14] G.Q. Xie, F.X. Qin, S.L. Zhu, and A. Inoue, Ni-free Ti-based bulk metallic glass with potential for biomedical applications produced by spark plasma sintering, *Intermetallics*, 29(2012), p. 99.

[15] I. Thibon, D. Ansel, M. Boliveau, and J. Debuigne, Interdiffusion in the β Mo-Ti solid solution at high temperatures,

*Mater. Res. Adv. Tech.*, 89(1998), p. 187.

[16] L. Feng, J.S. Li, L. Huang, H. Chang, Y.W. Cui, and L. Zhou, Interdiffusion behavior of Ti–Mo binary system in β phase, *Chin. J. Nonferrous Met.*, 19(2009), No. 10, p. 1766.

[17] L. Bolzoni, P.G. Esteban, E.M. Ruiz-Navas, and E. Gordo, Mechanical behaviour of pressed and sintered titanium alloys obtained from prealloyed and blended elemental powders, *J. Mech. Behav. Biomed. Mater.*, 14(2012), p. 29.

[18] P. Majumdar, S.B. Singh, and M. Chakraborty, The role of heat treatment on microstructure and mechanical properties of Ti–13Zr–13Nb alloy for biomedical load bearing applications, *J. Mech. Behav. Biomed. Mater.*, 4(2011), No. 7, p. 1132.

[19] E. Delvat, D.M. Gordin, T. Gloriant, J.L. Duval, and M.D. Nagel, Microstructure, mechanical properties and cytocompatibility of stable beta Ti–Mo–Ta sintered alloys, *J. Mech. Behav. Biomed. Mater.*, 1(2008), No. 4, p. 345.

[20] A. Almeida, D. Gupta, C. Loable, and R. Vilar, Laser-assisted synthesis of Ti–Mo alloys for biomedical applications, *Mater. Sci. Eng. C*, 32(2012), No. 5, p. 1190.

[21] M. Niinomi, M. Nakai, and J. Hieda, Development of new metallic alloys for biomedical applications, *Acta Biomater.*, 8(2012), No. 11, p. 3888.

[22] Y.L. Zhou and D.M. Luo, Microstructures and mechanical properties of Ti–Mo alloys cold-rolled and heat treated, *Mater. Charact.*, 62(2011), No. 10, p. 931.

[23] F. Geng, M. Niinomi, and M. Nakai, Observation of yielding and strain hardening in a titanium alloy having high oxygen content, *Mater. Sci. Eng. A*, 528(2011), No. 16-17, p. 5435.